Renormalization-group study of a concentrated fluctuating-valence model

W. Hanke* and J. E. Hirsch
Institute for Theoretical Physics, University of California, Santa Barbara, California 93106
(Received 4 December 1981)

The ground state and gap properties of a spinless model of f and d electrons with hybridization V and f-d interaction U_{fd} are studied in one dimension using a real-space renormalization-group (RG) method. To understand the dependence of the RG results on the cell size chosen, we first study the problem for $U_{fd}=0$ and arbitrary cell size N. It is found that even-site cells give qualitatively incorrect results for the gap, while odd-site cells (as small as $N=3$) reproduce very accurately the exact results for the gap and give a reasonable upper bound for the ground-state energy. On the basis of this result the phase diagram is studied as a function of arbitrary V and U_{fd} using three site cells. We consider the half-filled band situation for which the ground state is found to be insulating for all values of $U_{fd}(\neq 0)$. The f-electron occupation number as a function of E_f changes continuously, confirming recent mean-field results. This result indicates that the interacting f-d system does not scale to a single impurity model as argued in previous studies. Using a Jordan-Wigner transformation from spin to fermion operators, the Kondo necklace model is mapped onto a fluctuating valence model and the transition from ferromagnetic to Kondo-state behavior is numerically studied using $N=3$.

I. INTRODUCTION

Fluctuating valence (FV) materials present a challenge to modern many-body theory. Whereas most interacting many-body systems can be successfully described in terms of the standard perturbation theory based on an expansion in powers of the Coulomb interaction, using the Feynman-Dyson diagram scheme, the physics of FV systems dictates a different approach: the characteristic and unique features of FV materials such as SmS result from the fact that two profoundly different states of a rare-earth ion, one with electronic configuration f^n as in the free atom and the other with f^{n-1} plus one conduction electron, can be nearly degenerate in the solid-state environment.[1] The f electrons themselves remain deeply inside the core and strongly interact with each other (with interaction energies of the order of ~ 10 eV) and with the band of predominantly d-type electrons (interaction energies ~ 1 eV). Thus, one has to deal simultaneously with extremely localized atomic states and delocalized band states near the Fermi level. The usual Feynman-Dyson scheme[2] therefore is inappropriate, as the strong local correlations dominate the single-particle kinetic terms describing f-to-band electron transfers between atoms. Even though these kinetic terms may be small compared to the interaction terms, at low temperatures the standard perturbation expansion in these terms becomes divergent because of the large degeneracies (configurational degeneracies of the f^{n-1} levels) and quasidegeneracies (of f^{n-1} and f^n plus conduction electron) involved.

A tool developed for the analysis of such divergences and the extraction of the underlying physics is the renormalization-group (RG) method.[3,4] This technique has already been successful in resolving the physics of single-impurity models of FV systems,[5-7] in which the interactions between the rare-earths atoms, embedded in a homogeneous electron gas of ("d") band electrons are neglected. These single-impurity studies, in particular the most advanced numerical RG study of Krishna-Murthy *et al.*, give in principle a valid description of a very dilute system of transition-metal- or rare-earth-type atoms in a simple metal. Here the configurational degeneracy of the impurity atoms is lifted by the transfer term which introduces valence fluctuations. On the other hand, recent mean-field results on the nature of the FV phase transition[8] indicate significant (first- versus second-order) differences if the "concentrated" case of interacting impurities is considered.

In the present work a real-space renormalization-group technique is used to study the ground-state and low-excitation (in particular gap) properties of two rather simplified, however "concentrated" models of a FV system.[9] The method[10] consists of an iterative, approximate construction of the low-lying states of these model systems. The lattice is split into blocks which are solved exactly. A few low-lying block eigenstates are retained to rewrite the intra- and interblock terms, and the scheme is repeated until it converges to a "fixed point." Our first model emphasized the charge fluctuation aspects and neglects spin dynamics, whereas the second one (Kondo-lattice model) concentrates on spin couplings and

neglects charge-density interactions.

The first one is a two-band system of f and d electrons with hybridization V and f-d Coulomb interaction U_{fd}, with a Hamiltonian

$$H = E_d \sum_i d_i^\dagger d_i - t \sum_i (d_i^\dagger d_{i+1} + \text{H.c.}) + E_f \sum_i f_i^\dagger f_i + V \sum_i (f_i^\dagger d_i + \text{H.c.}) + U_{fd} \sum_i n_{d_i} n_{f_i} \ . \tag{1.1}$$

Here $d_i^\dagger$ creates a "d" electron state at site i with hopping probability $-t$, and $f_i^\dagger$ creates an "f" state with local energy E_f. t defines the scale of energies and is set $=1$ in what follows. In this one-dimensional model the orbital dynamics are simplified by using s instead of f and d states, resulting in a simple form of local interactions. Furthermore, it neglects spin degree of freedom and the Hubbard correlation term U_{ff}. They are essential for the study of magnetic properties of FV compounds, in particular for the commonly observed Kondo-like quenching of local f moments at low temperatures as discussed in the second model. Nevertheless, the spinless model in Eq. (1.1) shows some of the main characteristics encountered in FV systems, i.e., the quasidegeneracies of two ionic states, as well as the difficulties with perturbative approaches. It also displays within mean field[8] the indicated difference in the nature of the FV phase transition (continuous–discontinuous) depending on whether the "concentrated" or "single-impurity" system is considered. This difference, which is probably not changed by inclusion of spin, is one of the main issues which we want to address and clarify with this study.

In a recent paper Schlottmann[11] has studied the same model using multiplicative RG methods[12] which can be justified, only for U and V small compared to the bandwidth. He finds a distinction between $U_{fd} << V$ and $U_{fd} >> V$ regimes, with the latter corresponding to a system of isolated impurities in a Fermi sea and displaying a discontinuity in the f occupation number as a function of E_f.

One objective of our work is a study of the f-d model in Eq. (1.1) at zero temperature for the entire (U_{fd}, V) phase diagram, without a restriction to small parameters U_{fd} or V. Our results do not give a basis for a distinction between small and large U_{fd} regimes: they show that the scaling is always towards a "localized state" which is partly f and partly d in character and not towards a localized f level embedded in an extended d band (single-impurity model).

Another interesting aspect of the Hamiltonian (1.1) is the possibility of a metal-insulator transition which, according to mean-field studies by Falicov and coworkers,[13] can be driven by the electron-hole attraction $-U_{fd} n_d (1 - n_f)$ as a function of temperature (and thus electron and hole population). A finite temperature calculation will be the subject of a forthcoming paper. At $T=0$ K the metal-insulator transition in our RG results does not occur and we find for finite V and U a fixed-point Hamiltonian H^* with a hybridization ($E_f^* \neq E_d^*$) and Coulomb ($U^* \neq 0$) gap. However, these results are strongly related to the fact that we consider here only the half-filled band situation with, when averaged in the ground state, one electron per site. Extensions to non-half-filled-band cases where one starts from a metal, and where U_{fd} may introduce a Coulomb gap, will also be considered in a forthcoming paper.

The second model which we study is the "Kondo necklace" model introduced by Jullien *et al.*[14] for the description of the critical behavior of a concentrated system of magnetic Kondo impurities. This model can be derived from a model Hamiltonian very similar to Eq. (1.1) by a Jordan-Wigner transformation replacing fermion by spin operators, and results in one localized Kondo impurity spin per site, interacting antiferromagnetically with the conduction electron spins. As in previous block RG studies with two sites per block[14] we find a transition where the magnetism of the localized spins is destroyed by the formation of a singlet state with the conduction-electron spins.

The paper is organized as follows: after discussing in Sec. II the basics of the RG method, we demonstrate in Sec. III that the real-space RG method, with an appropriate choice of low-lying states kept in the iterations, is capable of reproducing very accurately ground-state and excited-state (gap) properties of the exactly solvable free fermion ($U_{fd}=0$) model. This exercise presents a valuable testing ground and illustrated the ability of the real-space approach to reproduce inherently $\vec{k}$ space related features of a two-component fermion system. It also gives a systematic procedure for choosing odd-site blocks to conserve internal symmetry (parity) and to produce correct gap results. In Sec. IV the general situation for $U_{fd} \neq 0$ is discussed on the basis of RG results with $N=3$ sites per block as a function of U_{fd}, V, and E_f. Ground state, gap properties, f-electron occupation, and localization length {behaving like a $[\exp(-bt/U_{fd})]$ for small U_{fd}/t} are calculated. In Sec. V the "Kondo necklace" model is mapped onto a FV model and the transition from antiferromagnetic to Kondo-state behavior is studied, again for $N=3$. Summarizing remarks are given in Sec. VI.

II. DESCRIPTION OF THE METHOD

The method we employ is a well-known nonperturbative RG technique for quantum systems. It consists of dissecting the lattice into small blocks, each containing a few (say N) sites, which are coupled to one another by the link terms [$\sim t$ in Eq. (1.1)] in

the Hamiltonian. A new effective Hamiltonian is constructed by computing the matrix elements of the original Hamiltonian in the space of states spanned by the eigenvectors having the lowest-energy eigenvalues in each block. The process is then repeated for the new effective Hamiltonian, whose coupling parameters change at each step. The procedure is iterated until reaching a regime that can be solved trivially or by perturbation theory. The iterations usually bring the Hamiltonian quickly to a "fixed-point" form. This form of the RG method has been employed for quantum field theories on a lattice[10] and for interacting spin (for example, the "Kondo necklace" model[14]) and electronic (the Thirring model[15] and the Hubbard model[16,17]) systems.

Consider the Hamiltonian in Eq. (1.1) with the chemical potential adjusted in such a way that the ground-state average of the site occupation $\langle n_f \rangle + \langle n_d \rangle = 1$ (half-filled-band case). Our Hilbert space has four states per site, denoted by $|0\rangle$, $|+\rangle$, $|-\rangle$, and $|+-\rangle$. We have the freedom of working with the d and f electronic states, as in the Hamiltonian (1.1), or with a site-diagonalized representation, making use of the canonical transformation

$$c_{i,-} = \alpha d + \beta f \ , \quad c_{i,+} = \beta d - \alpha f \ , \tag{2.1}$$

where $\alpha^2 + \beta^2 = 1$ ($\alpha = \beta = \frac{1}{2}$, for $E_d \equiv E_f$). In the latter representation, with

$$c_{i,-}^\dagger |0\rangle = |-\rangle_i, \quad c_{i,+}^\dagger |0\rangle = |+\rangle_i \ , \quad c_+^\dagger c_-^\dagger |0\rangle = |+-\rangle_i \tag{2.2}$$

and after reexpressing on-site and hopping terms of Eq. (1.1) in the basis (2.2), we arrive at an equivalent new form for the starting Hamiltonian which no longer contains explicitly the hybridization V

$$H = \sum_i (E_+ n_{i,+} + E_- n_{i,-} + E_{+-} n_{i,+} n_{i,-}) - t \sum_i [(c_{i,+}^\dagger + c_{i,-}^\dagger)(c_{i+1,+} + c_{i+1,-}) + \text{H.c.}] \ . \tag{2.3}$$

In the first step of the RG procedure, the chain is decomposed into N-site blocks as in Fig. 1, which are coupled together through the hopping term proportional to $(-t)$ in Eq. (1.1) or in Eq. (2.3). The Hamiltonian for each block is then exactly diagonalized by making use of the good quantum numbers, in our example the number of particles per block and parity. For $N=2$ sites per block, for example, the largest matrix (only in the $N-1$, parity $\equiv -1$ subspace) encountered in solving the eigenvalue problem in 4×4. With all other matrices being 3×3 or smaller the $N=2$ sites-per-block problem can easily be solved analytically and the RG equations derived. The $N=3$-sites-per-block problem is somewhat more tedious and has been carried out on a computer making use of efficient diagonalization procedures.

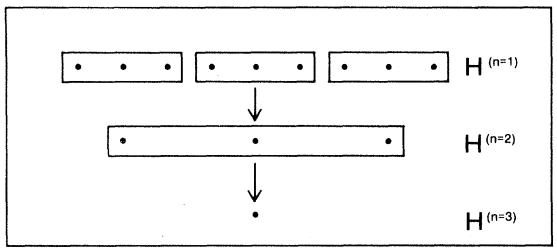

FIG. 1. Schematic picture of the block RG procedure.

The second step consists in "freezing out" higher-energy block states, since we are only interested in ground-state and low-excitation properties of the Hamiltonian (1.1). Since the calculation is restricted to the average occupation $\langle n_f \rangle + \langle n_d \rangle = 1$, the chemical potential is chosen so that the lowest-energy state satisfies that condition. We keep the $m=4$ lowest-energy states of the 4^N block states ($N=3$ gives 64 states), with the two lowest states stemming from the N-particle subspace, denoted again by $|+\rangle^{(1)}$ and $|-\rangle^{(1)}$. The other two states come from the lowest states of the $(N-1)$-particle subspace ($|0\rangle^{(1)}$) and the $(N+1)$-particle subspace ($|+-\rangle^{(1)}$). The choice of keeping only four lowest states is partly dictated by noting that these four states resemble the original site states in their occupation number if we subtract two from the particle number in the new states. This choice will be further substantiated in Sec. III. It guarantees that the new Hamiltonian $H^{(1)}$ is of the same form as the starting one in Eq. (2.3) if we now proceed to the third step and reexpress the Hamiltonian in the new basis of these four lowest states. After n iterations, one thus maintains a Hamiltonian of general form (see also Fig. 1)

$$H^{(n)} = \sum_j (H_j^{(n)} + H_{j,j+1}^{(n)}) \ . \tag{2.4}$$

Here the intrablock Hamiltonian is given by

$$H_j^{(n)} = E_0^{(n-1)} |0^{(n-1)}\rangle \langle 0^{(n-1)}|_j + E_+^{(n-1)} |+^{(n-1)}\rangle \langle +^{(n-1)}|_j + E_-^{(n-1)} |-^{(n-1)}\rangle \langle -^{(n-1)}|_j + E_{+-}^{(n-1)} |+-^{(n-1)}\rangle \langle +-^{(n-1)}|_j \ , \tag{2.5}$$

where the four projection operators select the lowest-energy states in the Hilbert space of the $(n-1)$th diagonalization step. Defining new cell operators by the relations

$$c_{+,j}^\dagger |0^{(n-1)}\rangle = |+^{(n-1)}\rangle \ ,$$

where the four projection operators select the lowest-energy states in the Hilbert space of the $(n-1)$th diagonalization step. Defining new cell

operators by the relations

$$\begin{aligned} c^{\dagger}_{+,j}|0^{(n-1)}\rangle &= |+^{(n-1)}\rangle \ , \\ c^{\dagger}_{-,j}|0^{(n-1)}\rangle &= |-^{(n-1)}\rangle \ , \\ c^{\dagger}_{+,j}c^{\dagger}_{-,j}|0^{(n-1)}\rangle &= -c^{\dagger}_{-,j}c^{\dagger}_{+,j}|0^{(n-1)}\rangle = |+-^{(n-1)}\rangle \ , \end{aligned} \tag{2.6}$$

and making use of the identity representation

$$\begin{aligned} l_j = &|0^{(n-1)}\rangle\langle 0^{(n-1)}|_j + |+^{(n-1)}\rangle\langle +^{(n-1)}|_j \\ &+ |-^{(n-1)}\rangle\langle -^{(n-1)}|_j + |+-^{(n-1)}\rangle\langle +-^{(n-1)}|_j \ , \end{aligned} \tag{2.7}$$

we obtain the nth step intracell Hamiltonian $H_j^{(n)}$

$$\begin{aligned} H_j^{(n)} = &E_+^{(n)}c^{\dagger}_{+,j}c^{\dagger}_{+,j} + E_-^{(n)}c^{\dagger}_{-,j}c_{-,j} \\ &+ U^{(n)}n_{+,j}n_{-,j} + d^{(n)}l_j \ . \end{aligned} \tag{2.8}$$

The recursion relations for the energy parameters in Eq. (2.8) are given by

$$\begin{aligned} E_+^{(n)} &= E_+^{(n-1)} - E_0^{(n-1)} \ , \\ E_-^{(n)} &= E_-^{(n-1)} - E_0^{(n-1)} \ , \\ U^{(n)} &= E_{+-}^{(n-1)} + E_0^{(n-1)} - E_+^{(n-1)} - E_-^{(n-1)} \ , \\ d^{(n)} &= Nd^{(n-1)} + E_0^{(n-1)} \ , \end{aligned} \tag{2.9}$$

with the initial conditions $d^{(0)} = E_0^{(0)} \equiv 0$ [compare with the starting Hamiltonian $H \equiv H^{(0)}$ in Eq. (2.3)].

Precisely as in the original "site-diagonalized" Hamiltonian (2.3), the difference $\frac{1}{2}(E_+^{(n)} - E_-^{(n)})$ provides information about the splitting of the two lowest levels in the N-particle-per-block subspace due to hybridization and thus corresponds to a "hybridization gap." On the other hand $U^{(n)}$ measures the energy difference created by putting two particles on the same site and may be called a "Coulomb gap."

In order to construct the interblock Hamiltonian $H_{j,j+1}^{(n)}$ we have first to express the old [$(n-1)$th step] hopping operators on the left-hand and right-hand boundary sites of the block (see Fig. 1) in the reduced subspace of states $|0^{(n-1)}\rangle$, $|+^{(n-1)}\rangle$, etc. For example, the $(n-1)$th step operator $c_{+,i}$ is then replaced by

$$\begin{aligned} c_{+,i} = &\alpha_+|0^{(n-1)}\rangle\langle +^{(n-1)}|_j \\ &+ \beta_+|0^{(n-1)}\rangle\langle -^{(n-1)}|_j \\ &+ \gamma_+|+^{(n-1)}\rangle\langle +-^{(n-1)}|_j \\ &+ \delta_+|-^{(n-1)}\rangle\langle +-^{(n-1)}|_j \ , \end{aligned} \tag{2.10}$$

where

$$\begin{aligned} \alpha_+ &= \langle 0^{(n-1)}|c_{+,N}|+^{(n-1)}\rangle \ , \\ \beta_+ &= \langle 0^{(n-1)}|c_{+,N}|-^{(n-1)}\rangle \ , \text{ etc.} \end{aligned} \tag{2.11}$$

Similarly, the $(n-1)$th step operator $c_{+,i+1}$ is expanded as in Eq. (2.10), but with the matrix elements α_+, β_+ etc. calculated with the block-diagonalized states $|0^{(n-1)}\rangle_{,}|+^{(n-1)}\rangle$, etc. and the operator $c_{+,1}$ taken at the left-hand side of a block. Using then the expansion in new (nth step) cell operators

$$\begin{aligned} |0^{(n-1)}\rangle\langle +^{(n-1)}|_j &= c_{+,j}(1-n_{-,j}) \ , \\ |0^{(n-1)}\rangle\langle -^{(n-1)}|_j &= c_{-,j}(1-n_{+,j}) \ , \\ |+^{(n-1)}\rangle\langle +-^{(n-1)}|_j &= -c_{-,j}n_{+,j} \ , \\ |-^{(n-1)}\rangle\langle +-^{(n-1)}|_j &= c_{+,j}n_{-,j} \ , \end{aligned} \tag{2.12}$$

we arrive at the general form for the interblock Hamiltonian

$$H_{j,j+1}^{(n)} = -t\{[\lambda_1^{(n)}c^{\dagger}_{+,j} + \lambda_2^{(n)}c^{\dagger}_{-,j} + (\lambda_4^{(n)} - \lambda_1^{(n)})c^{\dagger}_{+,j}n_{-,j} + (\lambda_2^{(n)} - \lambda_3^{(n)})c^{\dagger}_{-,j}n_{+,j}] \times (\text{ident. form})^{\dagger}_{j+1} + \text{H.c.}\} \tag{2.13}$$

with the initial conditions [see Eq. (2.3)] $\lambda_4^{(0)} = \lambda_1^{(0)} \equiv \beta$ and $\lambda_3^{(0)} = \lambda_2^{(0)} = \alpha$. Thus, in general, the $\lambda_1^{(n)}$, $\lambda_2^{(n)}$, etc. are obtained by calculating all the matrix elements of the old [$(n-1)$th step] hopping operator contained in the curly brackets of Eq. (2.10) on the boundary sites of the block between the states $|0^{(n-1)}\rangle$, $|+^{(n-1)}\rangle$, etc., and then collecting the terms proportional to one of the new (nth step) operators according to the prescription in Eq. (2.12). This finally defines the recursion relations for the hopping.

If one starts with a chain of N_{tot} sites, the chain after the first iteration has N_{tot}/N sites. Thus, after a few iterations n, we have constructed the ground and low-lying excited states of a very long chain (for $n = 7: N_{\text{tot}} = 3^7 = 2187$ sites). Effectively, the RG method therefore replaces the impossible diagonalization of a $4^{2187} \times 4^{2187}$ matrix by an approximate iterative procedure solving seven times a $4^3 \times 4^3$ block Hamiltonian matrix (which can be further reduced making use of conserved quantities). Typically, the calculation converges for the f-d problem within 7–10 iterations (except for very small U_{fd}). The physical meaning of a "fixed point" of the RG transformation is then that the physics contained in $H^{(n)}$ is no longer changed when "diagonalizing" in the $(n+1)$th step, a system which is a factor N larger. Finally, the ground-state energy density ϵ_0 is extracted out of the RG equations by noting that the constant $d^{(n)}$ in Eqs. (2.8) and (2.9) is the only parameter in the Hamiltonian which increases by a

power N for each iteration, and therefore scales with the volume of the system. It is thus given by

$$\epsilon_0 = \lim_{n\to\infty} (d^{(n)}/N^n) \ . \tag{2.14}$$

III. FREE-FERMION MODEL ($U_{fd}\equiv 0$)

Here we want to study the RG treatment of the exactly solvable free-fermion f-d two-band model. This provides an analytically solvable and critical test of the method. In particular, we want to demonstrate that not only ground-state but also low-excitation (gap) properties can be very accurately reproduced (including the correct analytical behavior for the hybridization gap) with a proper choice of low-lying block states and number N of block sites.

Consider the Hamiltonian (1.1) with $U_{fd}=0$, giving rise to an energy-band scheme as indicated in Fig. 2. In k representation we have

$$H = \sum_k [\epsilon_k d_k^\dagger d_k + V(d_k^\dagger f_k + \text{H.c.})] \ , \tag{3.1}$$

where

$$\epsilon_k = -2t\cos k \ , \tag{3.2}$$

and

$$k_l = \frac{\pi l}{N+1} \quad (1\le l\le N) \ , \tag{3.3}$$

denoting the k points in the Brillouin zone for a fixed choice of block sites N. The operators are

$$\begin{aligned} d_k &= (2/N+1)^{1/2}\sum_i \sin(kR_i)\, d_i \ , \\ f_k &= (2/N+1)^{1/2}\sum_i \sin(kR_i)\, f_i \ . \end{aligned} \tag{3.4}$$

The Hamiltonian (3.1) can be diagonalized, introducing $|\alpha_k\rangle$ and $|\beta_k\rangle$ one-particle states (for simplicity of notation we write down here only the $E_d\equiv E_f$ case)

$$\begin{aligned} \alpha_k^\dagger &= (d_k^\dagger + a f_k^\dagger)[1+a^2(k)]^{-1/2} \ , \\ \beta_k^\dagger &= (-a d_k^\dagger + f_k^\dagger)[1+a^2(k)]^{-1/2} \ , \end{aligned} \tag{3.5}$$

with energies

$$\epsilon_{\alpha,\beta}(k) = \frac{\epsilon_k}{2} \mp [(\epsilon_k/2)^2 + V^2]^{1/2} \ , \tag{3.6}$$

and normalization

$$a(k) = -[\epsilon_k + (\epsilon_k^2 + 4V^2)^{1/2}]/2V \ , \tag{3.7}$$

with the result

$$H = \sum_k [\epsilon_\alpha(k)\alpha_k^\dagger\alpha_k + \epsilon_\beta(k)\beta_k^\dagger\beta_k] \ . \tag{3.8}$$

α denotes the lower and β the upper band as in Fig. 2. From Eq. (3.6) the behavior of the hybridization gap E_G in the exact solution ($N\to\infty$) is

$$E_G = \lim_{N\to\infty} [\epsilon_\beta(k_1) - \epsilon_\alpha(k_N)] \sim \begin{cases} V, & V \gg 1 \\ V^2/t, & V \ll 1 \end{cases} . \tag{3.9}$$

We next have to introduce an appropriate choice of sites N and lowest states in the RG transformation. It has been pointed out by Drell *et al.*[15] that for a single-band fermion model (or a two-band model with identical bands) the low-lying energy levels of an even-site cell do not resemble the energy-level structure of a single site, and thus they advocate taking odd-site cells. Rabin[18] has studied the possibility of choosing even-site cells and mapping the model onto a more general model after the first RG iteration, but has shown that this can lead to spurious behavior. For our problem, the inadequacy of even-site cells is not completely obvious, since the four lowest energy states *are* separated by a gap from the rest of the cell states for both even and odd cells. Nevertheless, we will see that the rule of thumb that fermions require odd-site cells seems to hold for this case too.

The simplest case to consider is $N=2$ sites per block. For this case one can analytically derive the RG equations for general V and $U_{fd}\neq 0$. The result of this exercise is a phase diagram in the (U,V) plane which everywhere displays a gap between ground- and next-lowest excited state, with the exception of a parabolically shaped regime for small U_{fd} and $V\lesssim 0.4$ where the system becomes a metal. This finding is clearly in contradiction to the exact result for $U_{fd}=0$ [see Eq. (3.8)], which gives always a hybridization gap for $V\neq 0$.

For arbitrary N, the four lowest-lying states are given in the momentum-space description of Eq.

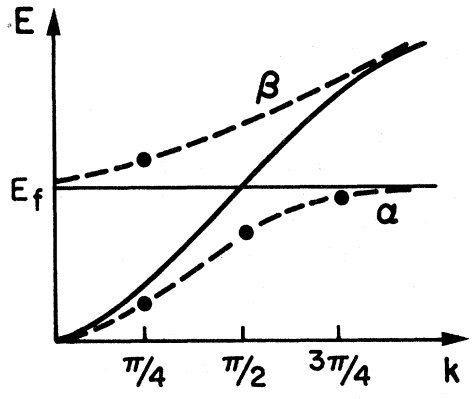

FIG. 2. Single-particle states for a three-site cell in the two-band model.

(3.8) by

$$|0^{(1)}\rangle=\prod_{l=1}^{N-1}\alpha_{k_l}^{\dagger}|0\rangle,\quad |+^{(1)}\rangle=\beta_{k_1}^{\dagger}|0^{(1)}\rangle$$
$$|-^{(1)}\rangle=\alpha_{k_N}^{\dagger}|0^{(1)}\rangle,\quad |+-^{(1)}\rangle=\beta_{k_1}^{\dagger}\alpha_{k_N}|0^{(1)}\rangle \tag{3.10}$$

Thus, the lowest state $|-^{(1)}\rangle$ corresponds to having the α band full, whereas the next-lowest state $|0^{(1)}\rangle$ is with the α band full except for the state with largest $k\equiv k_N$, etc. The states in Eq. (3.10) define the new intrablock Hamiltonian $H_j^{(1)}$ as in Eq. (2.8).

From this the new hybridization follows

$$\begin{aligned}V^{(1)}=(E_{+}^{(1)}-E_{-}^{(1)})/2&=\epsilon_\beta(k_1)-\epsilon_\alpha(k_N)\ ,\\&=-t\cos(\pi/N+1)\\&\quad+[t^2\cos^2(\pi/N+1)^2+V^2]^{1/2}\end{aligned} \tag{3.11}$$

which is already proportional to V^2/t or V, for $V\gg 1$ or $V\ll 1$, respectively. For the new intercell coupling we need to express the operators d_1 and d_N on the block boundaries in terms of the operators α_k and β_k:

$$\begin{aligned}d_1&=\left[\frac{2}{N+1}\right]^{1/2}\sum_{l=1}^{N}\sin\frac{\pi l}{N+1}[1+a^2(k)]^{-1/2}[\alpha_{k_l}-a(k_l)\beta_{k_l}]\ ,\\ d_N&=\left[\frac{2}{N+1}\right]^{1/2}\sum_{l=1}^{N}\sin\frac{\pi Nl}{N+1}[1+a^2(k_l)]^{-1/2}[\alpha_{k_l}-a(k_l)\beta_{k_l}]\ .\end{aligned} \tag{3.12}$$

As described in Sec. II [Eqs. (2.10) and (2.11)], we then have to calculate the matrix elements α_+, β_+, γ_+, and δ_+ of d_1 and d_N between the four lowest block states as defined in Eq. (3.10). After this straightforward exercise, and making use of the expansion (2.12) in new cell operators, we find

$$\begin{aligned}d_1&=\lambda(c_{+}^{(1)}+c_{-}^{(1)})=\sqrt{2}\lambda\tilde{c}_{+,j}\ ,\\ d_N&=\lambda[c_{+}^{(1)}+(-1)^{N+1}c_{-}^{(1)}]=\sqrt{2}\lambda\tilde{c}_{\pm,j}\ ,\end{aligned} \tag{3.13}$$

where we have defined canonical cell operators $\tilde{c}_+$ and $\tilde{c}_-$, and

$$\lambda=\left[\frac{2}{N+1}\right]^{1/2}\sin\left[\frac{\pi}{N+1}\right]\frac{1}{[1+a^2(k_N)]^{1/2}}\ . \tag{3.14}$$

We note that, for even N, the parity of the new cell states changes after every iteration step. The new intercell coupling follows from

$$H_{j,j+1}^{(1)}=-t[d_N^{\dagger}(j)d_1(j+1)+\text{H.c.}] \tag{3.15}$$

as

$$t^{(1)}=2t\lambda^2\ . \tag{3.16}$$

Extracting from Eqs. (3.11), (3.14), and (3.16) the ratio of the new hybridization to the new linking to lowest order in V, we find

$$V^{(1)}/t^{(1)}=(N+1)\left[2\cos\left[\frac{\pi}{N+1}\right]\tan^2\left[\frac{\pi}{N+1}\right]\right]^{-1} \tag{3.17}$$

or, for

$$\begin{aligned}&N=2:\ V^{(1)}/t^{(1)}=1\ ,\\ &N=3:\ V^{(1)}/t^{(1)}=2.83\ .\end{aligned} \tag{3.18}$$

This result already indicates in the first iteration one further difficulty with a two-sites-per-block model: with $t^{(1)}$ [from Eq. (3.14), $\lambda\sim V/t$, to lowest order] being proportional to V^2/t and thus very small, $V^{(1)}$ for the $N=2$ case is pushed to a similar very small value. When further iterated this process continues, finally converging into a vanishing hybridization gap E_G for small but finite V, in contrast to the exact result. The construction in Fig. 2 for the hybridized bands gives also some indication about why the $N=2$ case cannot reproduce the gap properties: for $N=2$ only two momenta, $k_1=\pi/3$ and $k_2=2\pi/3$, are used to construct the four lowest states. Thus, the most important region for hybridization around $k=\pi/2$ is left out. However, this is not so for odd-site cells, starting from $N=3$ with $k_1=\pi/4$, $k_2=\pi/2$, and $k_3=3\pi/4$.

The recursion relations for arbitrary N can be derived immediately by noting that $H^{(1)}$ is again of the same form as our starting Hamiltonian in Eq. (3.1) and simply repeating the above construction. The general case with $E_d\neq E_f$ follows step by step the above procedure.

The result for the energy gap, defined as $E_G=(E_{+}^{(n)}-E_{-}^{(n)})/2$, as a function of V/t is compared in Fig. 3 for the $N=3$ case with the exact result. We get analytically the correct limiting behavior with E_G being proportional to V or V^2/t for large and small V [as in Eq. (3.9)]. Also the magnitude is in very good agreement with the exact behavior. The $N=5$-sites-per-block calculation is already indistinguishable from the exact result for the gap on the scale of Fig. 3. In Fig. 4 we compare the

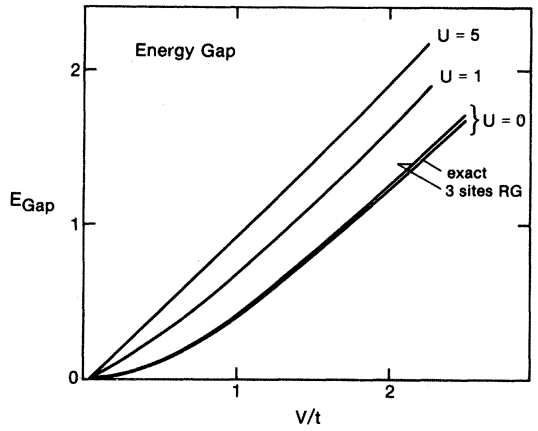

FIG. 3. The hybridization gap $E_G=(E_+^*-E_-^*)/2$ from the RG calculations. All calculations are with $N=3$ sites per block.

exact result for the ground-state energy density

$$\epsilon_0=\frac{1}{N}\sum_k \epsilon_\alpha(k)=-\frac{V}{\pi}\int_0^\pi dk[1+t^2\cos^2 k/V^2]^{1/2} \ , \tag{3.19}$$

with the RG calculation results for $N=3$ and $N=5(u_{fd}=0)$. The ground-state energy is derived by iteration, i.e., having in the first step

$$E_0^{(1)}=\sum_{l=1}^{N-1}\epsilon_\alpha(k_l)\equiv C(V,t) \ , \tag{3.20}$$

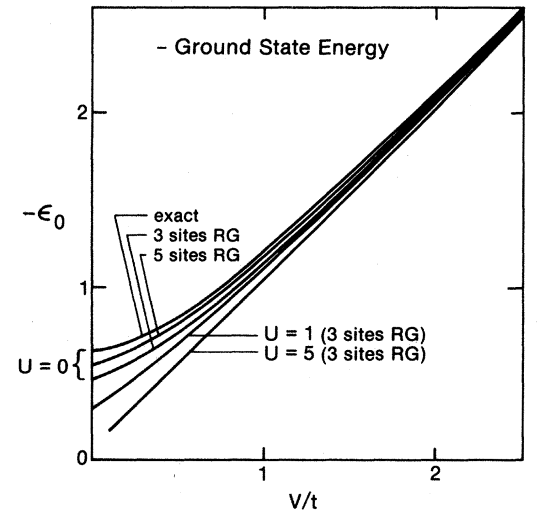

FIG. 4. Ground-state energy from the RG calculations for $U_{fd}=0$ and $N=3$, $N=5$ sites per cell, and for $U_{fd}=5$, $U_{fd}=1$ for $N=3$.

and in the second and third

$$E_0^{(2)}=\langle 0^{(2)}|H^{(1)}|0^{(2)}\rangle=NE_0^{(1)}+C(V^{(1)},t^{(1)}) \ , \tag{3.21}$$

$$E_0^{(3)}=N(NE_0^{(1)})+C(V^{(1)},t^{(1)})+C(V^{(2)},t^{(2)}) \ , \text{ etc.}$$

Thus, for the energy density the recursion formula derives

$$\epsilon_0^{(n+1)}=\epsilon_0^{(n)}+C(V^{(n)},t^{(n)})/N^{n+1} \ . \tag{3.22}$$

We note in Fig. 4 that the overall agreement of the approximate ground-state energy with the exact result is quite good, in particular for $N=5$, and again the exact analytical behavior for $V>>t$ with $\epsilon_0\sim V$ is reproduced. For small V the deviations are larger and increasing for smaller block sizes.

Summarizing this section, we have found the RG analysis to work very accurately for the case of a free two-component fermion system when taking odd-site cells. Gap properties for small and large hybridization reproduce the exact analytical behavior. The value of this exercise lies in particular in providing a rational for a proper choice of sites N and lowest states kept in the block diagonalization procedure. On the basis of this result we can now tackle the general $U_{fd}\neq 0$ situation.

IV. RESULTS FOR ARBITRARY U_{fd}

The RG study for $N=3$ and general U_{fd} was done numerically, following the steps of Sec. II. Efficient diagonalization subroutines were used to construct the cell eigenstates from which the new Hamiltonian $H^{(n)}$ of the nth iteration step results. Typically, the procedure converges after $n=7$ to 10 steps.

The numerical results can be summarized as follows: if we start from $V\neq 0$ initially, the scaling is always towards a fixed-point Hamiltonian H^*, which is characterized by [see Eqs. (2.5) and (2.13)] a finite "hybridization gap"

$$E_+^*-E_-^*\neq 0 \ , \tag{4.1}$$

and vanishing intercell couplings

$$\lambda_1^*=\lambda_2^*=\lambda_3^*=\lambda_4^*=0 \ . \tag{4.2}$$

This includes $U=0$, which is therefore also a fixed point. If, furthermore, $U\neq 0$ initially, the fixed point is in addition characterized by a "Coulomb gap"

$$U^*\neq 0 \ . \tag{4.3}$$

Thus, we find the f-d model (1.1) always to scale towards a fixed-point Hamiltonian H^* with insulating behavior (except for $U=V=0$). Of course this finding is closely related to our choice of the half-filled

band case. Present extensions of this work are therefore directed to non-half-filled situations, starting from a metal, where the Coulomb interaction U_{fd} may introduce a metal-insulator transition. Another interesting extension is the $T \neq 0$ K situations. Here, a finite electron-hole population can give rise to an electron-hole attraction, $U_{fd} n_d (1 - n_f)$, which, according to mean-field studies,[13] can introduce an insulator-metal transition.

Figure 3 gives the results for the hybridization gap as a function of the initial hybridization V for the $U_{fd} = 1$ and $U_{fd} = 5$. We note that the gap is enhanced for larger Coulomb interaction. For very large $U_{fd} >> 1$, the hybridization gap E_G becomes again proportional to V, which is in accordance with the exact result [for $U_{fd} \to \infty$, every site is singly occupied, giving rise to $(E_+ - E_-) \sim V$].

Figure 4 displays the ground-state energy, which is of course enhanced for larger interaction U_{fd}. Also the ground-state energy for $U >> 1$ is proportional to V, again following the exact results [with every site being singly occupied, for $E_d = E_f = 0$, there is no hopping, and only the hybridization term in the Hamiltonian, Eq. (1.1), contributes].

Quantities which display different behavior in single versus concentrated fluctuating valence models are the shape and dependence of the f and d occupation number, $\langle n_f \rangle$ and $\langle n_d \rangle$ on the location of the total f energy E_f.

It has been shown by Leder,[8] within mean-field [self-consistent Hartree-Fock (HF)] approximation, that the Falicov-Kimball model extended by hybridization [Eq. (1.1)] always results for nonvanishing V in an occupation $\langle n_f \rangle$ which varies continuously with E_f. On the other hand, earlier mean-field calculations for this model[19] suggest that first-order phase transitions can still exist for finite hybridization. Closer inspection of this earlier work reveals, however, that here the one-particle Green's function for the f electrons is taken from the single-impurity model, resulting in a discontinuous solution of the Hartree-Fock equations for $\langle n_f \rangle$.[8]

The RG calculation of the ground-state expectation value of n_f proceeds very much along the lines of the analysis for H in Sec. II. Define the operator

$$\hat{n}_f = N^{-1} \sum_{i=1}^{N} f_i^\dagger f_i \ . \tag{4.4}$$

Then, compute the matrix elements of $\hat{n}_f$ between the new cell states $|0^{(1)}\rangle$, $|+^{(1)}\rangle$, $|-^{(1)}\rangle$, and $|+-^{(1)}\rangle$, denoted by a_0, a_+, a_-, and a_{+-}. As a result, we find [see also Eqs. (2.6) to (2.9)]

$$\begin{aligned} \hat{n}_f = {} & a_0 + (A_+ - a_0) |+^{(1)}\rangle \langle +^{(1)}| \\ & + (a_- - a_0) |-^{(1)}\rangle \langle -^{(1)}| \\ & + (a_{+-} - a_0) |+-^{(1)}\rangle \langle +-^{(1)}| \\ = {} & a_0 + (a_+ - a_0) n_+ + (a_- - a_0) n_- \\ & + (a_{+-} - a_+ - a_- + a_0) n_+ n_- \ . \end{aligned} \tag{4.5}$$

In the next step, write the recursion relations for the operators $|+^{(1)}\rangle\langle +^{(1)}|$, $|-^{(1)}\rangle\langle -^{(1)}|$, and $|+^{(1)}\rangle\langle +-^{(1)}|$ in Eq. (4.5). They can be arranged in matrix form, starting from

$$\begin{pmatrix} |+^{(1)}\rangle & \langle +^{(1)}| \\ |-^{(1)}\rangle & \langle -^{(1)}| \\ |+-^{(1)}\rangle & \langle +-^{(1)}| \end{pmatrix} = \begin{pmatrix} v_1 \\ v_2 \\ v_3 \end{pmatrix} + \begin{pmatrix} a_{11} & a_{12} & a_{13} \\ a_{21} & a_{22} & a_{23} \\ a_{31} & a_{32} & a_{33} \end{pmatrix} \begin{pmatrix} |+^{(2)}\rangle & \langle +^{(2)}| \\ |-^{(2)}\rangle & \langle -^{(2)}| \\ |+-^{(2)}\rangle & \langle +-^{(2)}| \end{pmatrix} \ , \tag{4.6}$$

or, when iterated

$$\vec{\omega} = \vec{v}_0 + \vec{A}_0 \cdot \vec{v}_1 + \vec{A}_0 \cdot \vec{A}_1 \cdot \vec{v}_2 + \cdots \ , \tag{4.7}$$

with the recursion relations

$$\vec{\omega}_{n+1} = \vec{\omega}_n + \vec{B}_n \cdot \vec{v}_n \ , \quad \vec{B}_{n+1} = \vec{B}_n \cdot \vec{A}_n \ . \tag{4.8}$$

The initial conditions are $\vec{B}_0 = \vec{1}$ and $\vec{\omega}_0 = 0$. Here

$$\begin{aligned} v_n(I) &= \langle 0^{(n+2)} || I \rangle \langle I || 0^{(n+2)} \rangle \ , \\ A_n(I,J) &= \langle J^{(n+2)} || I \rangle \langle I || J^{(n+2)} \rangle \ , \end{aligned} \tag{4.9}$$

with I and J standing for the states $+$, $-$ and $+-$.

Figure 5 gives the results for the ground-state expectation value $\langle n_f \rangle$ around the center of the d band as a function of f-d interaction for fixed hybridization $V = 0.1$. The valence transition from $E_f > 0$ to $E_f < 0$ is always continuous, and is in qualitative agreement with the mean-field results of Leder.[8] The

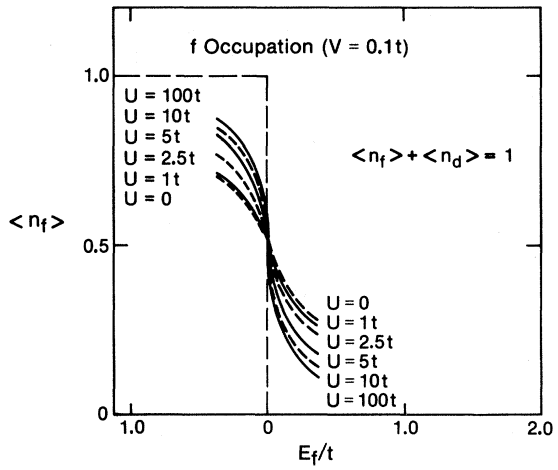

FIG. 5. Ground-state average of the f-electron occupation as a function of the f-level energy E_F for fixed hybridization $V = 0.1t$ and varying interaction U_{fd}.

slope is steeper for larger Coulomb interaction, also in accordance with mean field. Figure 6 displays the behavior of $\langle n_f \rangle$ for fixed $U_{fd}=5$ but varying hybridization V. The slope is steeper for smaller V, again in qualitative agreement with the HF results. However, the RG calculation always results in a smooth transition near $E_f=0$, and never gives the sharp, nearly discontinuous changes for very small V's of the mean-field study.[8]

Another interesting quantity containing important physical information is the "localization length" ξ. It is a measure of the extension of the electronic wave functions in the ground state and is related to the decay of the correlation function[16]

$$F(R)=\frac{1}{N}\sum_i \langle c_{i+R}^{\dagger} c_i \rangle \ , \tag{4.10}$$

where the c's stand for d and f operators of Eq. (1.1). The general behavior of this function for large Coulomb interaction U_{fd} can be derived from the following perturbation theoretical argument, in complete analogy to the half-filled Hubbard chain[16]: for infinite $U_{fd}=\infty$ all sites are singly occupied. For finite but very large U_{fd}, we can derive the ground state from a perturbation expansion in t/U_{fd} and calculate with it the correlation function $F(R)$. Since every t term in this expansion introduces a nearest-neighbor hopping, the nth neighbor correlation in $F(R=na)$ (with a the lattice parameter) implies that only in nth order perturbation $F(R=na)$ is nonvanishing. Thus,

$$F(R) \sim (t/U_{fd})^n \sim \exp[-R\,(\ln t)/U_{fd}] \sim \exp(-R/\xi) \ . \tag{4.11}$$

That is, $F(R)$ decays exponentially on a length scale

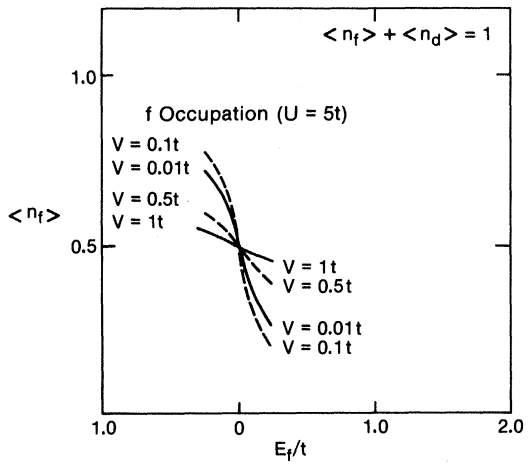

FIG. 6. Average occupation of f level as function of E_f for fixed interaction $U_{fd}=5t$ and varying hybridization V.

ξ in the insulating regime, where the above perturbation theory is convergent.

If the system behaves instead metallic with free-electron behavior, then it is easy to show[16] that $F(R)$ will display algebraic decay

$$F(R) \sim 1/R^{\eta} \ , \tag{4.12}$$

with η depending on the dimension and Fermi-surface topology.

We can derive an estimate of the correlation length near the insulator-metal transition from the following well-known argument: start the scaling with a small value of U_{fd}/t and assume, after n_0 iterations we have scaled to a "strong coupling regime" with $U_{fd}^{(n_0)}/\langle \lambda^{(n_0)} \rangle \gtrsim 1$, where $\langle \lambda \rangle$ is some average over the four intercell hopping constants of Eq. (2.13). This will happen when $\langle \lambda \rangle$ has scaled to a very small value, in which case the blocks will behave effectively as decoupled. The localization length will then be given approximately by the distance over which the nth iteration block extends, i.e.,

$$\xi \sim 3^{n_0} \tag{4.13}$$

in the $N=3$, three site per cell calculation. For small U_{fd}, we found (from our numerical RG analysis) the behavior of ξ to be

$$\xi \sim a \exp(b/U_{fd}) \ , \tag{4.14}$$

with a and b only weakly depending on the remaining parameters V and E_f. This behavior indicates that the Coulomb interaction term is a marginal operator. The Coulomb gap behaves as the inverse of the localization length

$$E_g \sim \exp(-b/U_{fd}) \ ,$$

which is the same behavior obtained in the Hubbard model from the exact solution.[20] However, there the real-space RG calculations[16,17] do not reproduce this exact analytic behavior [they give $E_g \sim \exp(-bt^2/U^2)$]. It would be interesting to shed some more light on the reason for this difference in the RG results for the two models.

Finally, we want to comment on some of our results when compared with those obtained by Schlottmann using the multiplicative RG technique.[11] In that work a different behavior emerges for the two regimes $U_{fd} \ll V$ and $U_{fd} \gg V$. For $U_{fd} \ll V$ the model of Eq. (1.1) is found to behave as "extended and coherent," which basically means that one has to treat the system as concentrated. On the other hand, for $U_{fd} \gg V$ the system behaves as "local and incoherent," and it is argued that each rare-earth ion behaves essentially as an isolated impurity. In this latter regime one would therefore be able to treat the system as a set of isolated impurities embedded in a Fermi sea of delocalized (the $d-$) states. Correspondingly, the ground-state expectation value of the

valence $\langle n_f \rangle$ changes discontinuously as a function of E_I.

These results of the perturbative RG analysis partly disagree with ours: from our analysis we find no justification for differentiating between the two regimes, $U_{fd} >> V$ and $U_{fd} << V$. As discussed above, our calculation yields a scaling which is always towards a "localized regime" on a length scale which is measured by the localization length ξ. However, there is an important difference to the "local and incoherent" picture of Schlottmann: our "localized regime" stems from a localized state that is partly f and partly d in character with, in particular, localization also occuring in the d states. In addition, as already mentioned above, we find the transition into the fluctuating valence regime to be continuous.

V. RELATION WITH THE CRITICAL BEHAVIOR OF THE KONDO NECKLACE FOR $N=3$

In this section we want to elaborate on the formal similarity between the two-component fermion model and a Kondo lattice model, the "Kondo necklace." One of the reasons to study this model arises from the anomalous electric resistivity and magnetic properties of many rare-earth compounds at low temperatures. For example, in the case of $CeAl_3$ the electrical resistivity curve increases with lowering temperature in the intermediate temperature range (100–50 K) and exhibits the characteristic $\ln T$ behavior as for isolated Kondo impurities. In addition, the low-temperature susceptibility is characteristic of a nonmagnetic ground state. This behavior may be the result of a quenching of the unpaired f-electron magnetic moment by correlation with the conduction-electron spins, again in complete analogy to the Kondo effect for isolated impurities. The need for a study of a concentrated system of impurities, the Kondo lattice, arises from the competing tendencies for the system to condense to a Kondo system with a vanishing gap, in which each f-electron moment is compensated by an associated conduction-band moment, or to order antiferromagnetically due to the Ruderman-Kittel-Kasuya-Yosida interaction. When the antiferromagnetic interaction J between conduction-electron spins and impurity spins is enhanced, a transition should occur from the magnetic state to the Kondo metal state.

Such systems may be modeled in one dimension by a straightforward generalization of the single spin s-d Hamiltonian to a periodic arrangement of the magnetic spins at each lattice site. The "Kondo necklace" (KN) introduced by Doniach[14] neglects the charge-density fluctuations originally contained in the Kondo lattice and only takes the spin degrees into account. It is defined by the Hamiltonian

$$H_{\mathrm{KN}} = J \sum_i \vec{S}_i \cdot \vec{\tau}_i + W \sum_i (\tau_i^x \tau_{i+1}^x + \tau_i^y \tau_{i+1}^y) \quad . \tag{5.1}$$

Here W denotes the conduction-band half-width and J the antiferromagnetic interaction between the spins of the conduction electrons and those of the impurities. $\vec{S}_i$ and $\vec{\tau}_i$ are the Pauli operators (the same for $\vec{\tau}_i$)

$$S_i^x = \begin{pmatrix} 0 & 1 \\ 1 & 0 \end{pmatrix}, \quad S_i^y = \begin{pmatrix} 0 & -i \\ i & 0 \end{pmatrix}, \quad S_i^z = \begin{pmatrix} 1 & 0 \\ 0 & -1 \end{pmatrix} \quad . \tag{5.2}$$

The main idea in that the model (5.1) has some analogy with the original Kondo lattice, in particular the crossover transition from an antiferromagnetic to "Kondo metal" state. However, whereas the real-space RG calculation by Jullien *et al.*[14] and also our RG analysis give a transition of a finite critical value J_c for the "Kondo necklace," a similar study for the Kondo lattice for a half-filled band gives a gap opening immediately when J is different from zero.[21] This is both reminiscent of the one-dimensional Hubbard model[16] and of the f-d model studied in this paper.

One can write the Kondo necklace Hamiltonian in terms of f and d fermion operators by using the following Jordan-Wigner transformations[22,23]

$$\tau_i^\dagger = d_i^\dagger \exp\left[-i\pi \sum_{j=1}^{i-1} n_{d,i} \right] \quad , \tag{5.3}$$

and

$$S_i^\dagger = f_i^\dagger \exp\left[-i\pi \sum_{j=1}^{i-1} n_{f,i} \right] \quad , \tag{5.4}$$

where $S_i^\dagger = S_i^x + iS_i^y$, $\tau_i^\dagger = \tau_i^x + i\tau_i^y$. The transformations in Eqs. (5.3) and (5.4) take care of the fact that the spin operators τ and σ anticommute on the same site, like Fermion operators, but commute on different sites.

Define

$$S_i^\dagger = a_{2i}^\dagger \quad , \quad \tau_i^\dagger = a_{2i+1}^\dagger \quad . \tag{5.5}$$

Then,

$$H = J \sum_i [(2n_{2i}-1)(2n_{2i+1}-1) + 2(a_{2i}^\dagger a_{2i+1} + a_{2i+1}^\dagger a_{2i})] + 2W \sum_i (a_{2i-1}^\dagger a_{2i+1} + a_{2i+1}^\dagger a_{2i-1}) \quad . \tag{5.6}$$

With the Jordan-Wigner transformation

$$a_i^\dagger = \exp\left[-i\pi \sum_{j=1}^{i-1} c_i^\dagger c_i \right] c_i^\dagger \quad ,$$

and (5.4) we find the term proportional to J in Eq.

(5.6) unchanged, whereas for the term proportional to W

$$a^{\dagger}_{2i-1}a_{2i+1}=\exp\left[-i\pi\sum_{j=1}^{2i-2}n_j c^{\dagger}_{2i-1}c_{2i+1}\exp\right]\left[i\pi\sum_{j=1}^{2i}n_j\right]=\exp(i\pi n_{2i})c^{\dagger}_{2i-1}c_{2i+1}=c^{\dagger}_{2i-1}c_{2i+1}(1-n_{2i})+n_{2i}(-c^{\dagger}_{2i-1}c_{2i+1}) \quad . \tag{5.7}$$

Therefore,

$$H_{\mathrm{KN}}=-2J_{\parallel}\sum_i(n_{d,i}+n_{f,i}) +2W\sum_i(d_i^{\dagger}d_{i+1}+\mathrm{H.c.})(1-2n_{f,i+1}) +2J_{\perp}\sum_i(d_i^{\dagger}f_i+\mathrm{H.c.})+4J_{\parallel}\sum_i n_{d,i}n_{f,i} \quad , \tag{5.8}$$

where we have used the definitions in Eqs. (5.3) to (5.5). With the initial conditions $J_{\parallel}=J_{\perp}=J$, $t=-2W$, $V=2J_{\perp}$, $J=-E_d/2$, and $U=2V$ the Kondo necklace therefore can be mapped onto the two-component fermion model of Eq. (1.1). There is, however, a slight modification in that a factor $(1-2n_{f,i+1})$ appears in the transfer terms. This factor, however, modifies the results substantially. As discussed in Sec. III, the $N=2$-sites-per-block calculation gives wrong results (metallic instead of insulating behavior) for small U_{fd} and V. This is due to the fact that in this case one misses the most important hybridization at $k=\pi/20$ in the middle of the B zone, and that internal symmetries (parity) are violated. In view of this fact it is quite surprising that already the $N=2$ RG calculation[14] gave a transition, which we also find in our $N=3$ study. The transition is from a degenerate ground-state characteristic of the magnetic state for $J/W<(J/W)_{\mathrm{crit}}=(V/t)_{\mathrm{crit}}=0.382$ to a singlet ground state which is characteristic of the Kondo state and which is separated by a gap $\Delta=2(J_{\perp}^{(n)})$ from the next excited state for $J/W>(J/W)_{\mathrm{crit}}$. The $N=2$ calculation in Ref. 14 with again four lowest states kept in the iterations gives for the critical ratio $(J/W)_{\mathrm{crit}}=0.411$, and with 16 states kept $(J/W)_{\mathrm{crit}}=0.375$. In mean field the $(J/W)_{\mathrm{crit}}$ value equals 1.[14] Figure 7 gives a plot of the gap Δ/W as function of J/W. For $(J/W)<(J/W)_{\mathrm{crit}}$, the system is equivalent to an XY model[21] with a magnetically degenerate ground state, where both neighboring $\vec{S}$ and $\vec{\tau}$ spins are found to be antiferromagnetically correlated.

Critical exponents have been evaluated at $(J/W)_{\mathrm{crit}}$. The critical index for the gap $\Delta=[(J/W)-(J/W)_{\mathrm{crit}}]^s$ is numerically extracted as $s=1.36$, appreciably larger than the $N=2$ result $s=1$.[14]

Finally, the ground-state energy found from our calculations (shown in Fig. 8) is lower than that obtained in Ref. 14 for $N=2$ with four lowest states kept, but somewhat higher than that of Ref. 14 when 16 lowest states per cell are kept in the iterations.

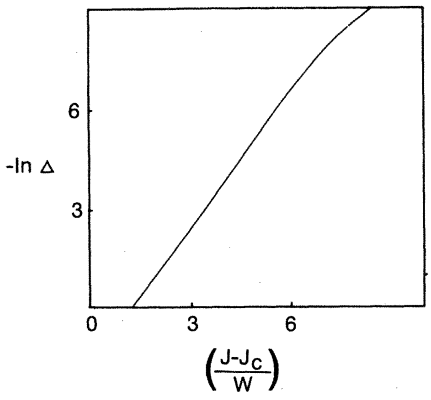

FIG. 7. Renormalization-group results on the Kondo necklace for $N=3$ sites per block: log-log plot of the gap as function of J/W.

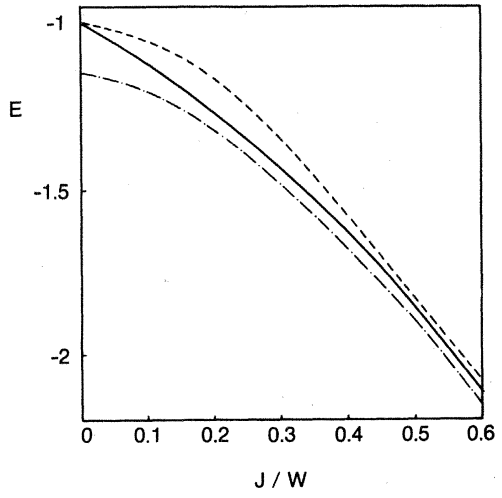

FIG. 8. Ground-state energy of the Kondo necklace model. Full line: this calculation ($N=3$). Dashed line: $N=2$ calculation with four states per cell (Ref. 14). Dash-dot line: $N=2$ with 16 states per cell (Ref. 14).

VI. SUMMARY

We have studied a one-dimensional model for a concentrated fluctuating valence solid using a real-space renormalization-group technique. The results presented in this paper are instructive both with respect to the method of calculation itself and to the physical properties of the model under consideration. Methodological questions were addressed in the study of the noninteracting case, $U_{fd}=0$, where exact results can be found and where the RG calculation can be carried out easily for arbitrary cell size. It was found that the method gives wrong results when using even site cells, as occurs in other models,[18] and some tentative reasons for this failure were given. For odd-site cells, the RG results for the gap were found to be very accurate even for three-site cells (better than 3% for all values of V), and the analytic behavior of the gap for small and large V was reproduced. The results for the ground-state energy were also reasonable. These results are very encouraging, since there is reason to believe that the method should be even better when Coulomb interaction is included and the states become more localized. On the basis of these results, the behavior of the model for nonzero U_{fd} was studied using an odd-number cell ($N=3$). The model was found to be insulating for any nonzero U, and the Coulomb gap was found to depend exponentially on the Coulomb interaction as in the Hubbard model. The fermion occupation number of f and d states was found to vary continuously with the parameters, confirming recent mean-field results.

Finally, a closely related model, the Kondo necklace, was studied using this technique with cell number $N=3$. The motivation for that study was the following: a previous RG study of this model using $N=2$ (Ref. 14) had found a transition from Kondo-quenched to antiferromagnetic behavior for a finite value of the coupling. However, in our fluctuating valence model we also found such a transition when taking $N=2$ which was, however, spurious, as it dissappeared when taking $N=3$. Nevertheless, in the Kondo necklace model we found the transition to persist for $N=3$, confirming the previous results by Jullien *et al.*,[14] with small modifications in the numerical values of the results.

We believe the results reported in this paper should encourage the study of more realistic models using these techniques, in particular the concentrated Anderson model including spin degrees of freedom.

ACKNOWLEDGMENTS

One of us (W.H.) would like to thank Dr. W. Kohn and the members of the Institute for Theoretical Physics where this work was done for the generous hospitality and support. The authors thank all members of the Intermediate Valence Workshop, including Dr. Falicov, Dr. Maple, and Dr. Kohn, for stimulating discussions. They acknowledge the help of Dr. J. Richardson, who gave them access to some of his computer routines and also advice with various computational aspects of this work. This work was supported by the National Science Foundation under Grant No. PHY77-27084 and through Max-Planck grants.

---

*Permanent address: Max-Planck Institut fur Festkorperforschung, D-7, Stuttgart, West Germany.

[1]For recent reviews, see: J. M. Jefferson and K. W. Stevens, J. Phys. 11, 3919 (1978); N. Grewe, H. J. Leder, and P. Entel, in *Festkorperprobleme XX,* edited by J. Treusch (Vieweg and Sohn, Braunschweig, 1980); and various articles in the *Proceedings of the International Conference on Valence Fluctuations in Solids,* edited by L. M. Falicov, W. Hanke, and M. B. Maple (North-Holland, Amsterdam, 1981).

[2]See, for example: A. L. Fetter and J. D. Walecka, *Quantum Theory of Many Particle System* (McGraw-Hill, New York, 1971).

[3]P. W. Anderson, J. Phys. C 3, 2436 (1970).

[4]K. G. Wilson, Rev. Mod. Phys. 47, 773 (1975).

[5]J. H. Jefferson, J. Phys. C 10, 3589 (1977).

[6]F. D. M. Haldane, Phys. Rev. Lett. 40, 416 (1978).

[7]H. R. Krishna-Murthy, J. W. Wilkins, and K. G. Wilson, Phys. Rev. B 21, 1003 (1980); 21, 1044 (1980).

[8]H. J. Leder, Solid State Commun. 27, 579 (1978).

[9]A preliminary short version of this work has been published in the conference proceedings of Ref. 1.

[10]S. D. Drell, M. Weinstein, and S. Yankielowicz, Phys. Rev. D 14, 1769 (1977).

[11]P. Schlottmann, Phys. Rev. B 22, 613 (1980); 22, 622 (1980).

[12]H. N. Menyhard and J. Solyom, J. Low Temp. Phys. 12, 529 (1973).

[13]R. Ramirez, L. M. Falicov, and J. C. Kimball, Phys. Rev. B 2, 3383 (1970).

[14]R. Jullien, J. N. Fields, and S. Doniach, Phys. Rev. B 16, 4889 (1977).

[15]S. D. Drell, B. Svetitsky, and M. Weinstein, Phys. Rev. D 17, 523 (1978).

[16]J. Hirsch, Phys. Rev. B 22, 5259 (1980).

[17]C. Dasgupta and P. Pfeuty, Phys. Rev. B 23, (1981).

[18]J. M. Rabin, Phys. Rev. B 21, 2027 (1980).

[19]D. I. Khomskii and A. N. Kochaijan, Solid State Commun. 18, 985 (1976).

[20]E. Lieb and F. Wu, Phys. Rev. Lett. 20, 1445 (1968).

[21]R. Jullien, P. Pfeuty, A. K. Bhattarcharjee, and B. Cogblin, J. Appl. Phys. 50, 7555 (1979).

[22]T. Jordan and E. Wigner, Z. Phys. 47, 631 (1928).

[23]E. Lieb, T. Schultz, and D. Mattis, Ann. Phys. (Paris) 16, 407 (1961).